PROCEEDINGS OF SPIE

SPIEDigitalLibrary.org/conference-proceedings-of-spie

A conceptual design study for Subaru ULTIMATE GLAO

François Rigaut, Yosuke Minowa, Masayuki Akiyama, Yoshito Ono, Visa Korkiakoski, et al.

François Rigaut, Yosuke Minowa, Masayuki Akiyama, Yoshito Ono, Visa Korkiakoski, Nick Herrald, Gaston Gausachs, Christophe Clergeon, Shiang-Yu Wang, Céline d'Orgeville, Jordan Davies, Yusei Koyama, Ikuru Iwata, Tadayuki Kodama, Kentrao Motohara, Yutaka Hayano, Ichi Tanaka, Takashi Hattori, Michitoshi Yoshida, "A conceptual design study for Subaru ULTIMATE GLAO," Proc. SPIE 10703, Adaptive Optics Systems VI, 1070324 (10 July 2018); doi: 10.1117/12.2314085

SPIE.

Event: SPIE Astronomical Telescopes + Instrumentation, 2018, Austin, Texas, United States

A conceptual design study for Subaru ULTIMATE GLAO

François Rigaut[a,*], Yosuke Minowa[b], Masayuki Akiyama[c], Yoshito Ono[b], Visa Korkiakoski[a], Nick Herrald[a], Gaston Gausachs[a], Christophe Clergeon[b], Shiang-Yu Wang[d], Céline d'Orgeville[a], Jordan Davies[a], Yusei Koyama[b], Ikuru Iwata[b], Tadayuki Kodama[c], Kentaro Motohara[f], Yutaka Hayano[e], Ichi Tanaka[b], Takashi Hattori[b], and Michitoshi Yoshida[b]

[a]Research School of Astronomy and Astrophysics, Australian National University, Canberra, ACT 2611, Australia
[b]Subaru Telescope, National Astronomical Observatory of Japan, 650 North Aohoku Place, Hilo, HI, 96720
[c]Astronomical Institute, Tohoku University, Aramaki, Aoba-ku, Sendai 980-8578, Japan
[d]Academia Sinica, Institute of Astronomy and Astrophysics, P. O. Box 23-141, Taipei, Taiwan
[e]National Astronomical Observatory of Japan, 2-21-1 Osawa, Mitaka, Tokyo, 181-8588, Japan
[f]Institute of Astronomy, University of Tokyo, 2-21-1 Osawa, Mitaka, Tokyo 181-0015, Japan

ABSTRACT

We report on the conceptual design study done for the Ground Layer Adaptive Optics system of the ULTIMATE-Subaru project. This is an ambitious instrument project, providing GLAO correction in a square field of view of 14 arcmin on a side, aiming to deliver improved seeing at the near infrared wavelength. Its client instruments are an imager and multi-IFU spectrograph at Cassegrain and a Multi-Object spectrograph at Nasmyth. In this paper, we introduce the ULTIMATE-Subaru project overview and its science case and report the results of the GLAO performance prediction based on the numerical simulation and conceptual design of the wavefront sensor system.

Keywords: adaptive optics, GLAO

1. INTRODUCTION

In the next decade, the Subaru telescope will offer unique wide-field imaging and spectroscopic capabilities at the prime focus using Hyper Suprime Cam[1] (HSC) and Prime Focus Spectrograph[2] (PFS). These instruments provide superb survey capabilities mainly in optical wavelength range and occupy the most of dark nights at the Subaru telescope. To further strengthen the wide-field capability of the Subaru Telescope, we have initiated the ULTIMATE-Subaru project since 2011. ULTIMATE-Subaru stands for Ultra-wide Laser Tomographic Imager and Multi-object spectrograph with AO for Transcendent Exploration by Subaru. We aim at developing wide-field near-infrared (NIR) imager and multi-object spectrograph (or IFU spectrograph) assisted by a ground-layer adaptive optics (GLAO) system as a new facility instrument of the Subaru telescope. The GLAO system will uniformly improve image quality over wide field of view ($14' \times 14'$) by correcting for the turbulence at the ground layer of the Earth's atmosphere. While our unique wide-field instruments (HSC and PFS) are optical instruments and they are operated in dark nights, ULTIMATE-Subaru will make full use of remaining bright nights of the Subaru Telescope in the 2020s. Based on our simulations (as described in Section 2 in more details), the ULTIMATE-Subaru GLAO system can provide FWHM$\sim$0.2 arcsec imaging quality over the $14' \times 14'$ field of view at K-band ($\lambda_c \sim 2.2\mu$m) under moderate seeing conditions at Maunakea. It is worth noting that the spatial resolution achieved by ULTIMATE-Subaru is comparable to that of the Hubble Space Telescope in NIR, as well as the future WFIRST mission which will be launched in mid 2020s. The improvement in the image quality will also enable to improve the sensitivity by a factor of $\sim 1.5 - 2.5$, which will greatly improve the survey power, particularly for faint compact sources in the distant universe. We published a study report[3] of the ULTIMATE-Subaru project in January 2016. This document summarizes science cases, AO/instrument design studies, as well as our development plans.

Send correspondence to François Rigaut: francois.rigaut@anu.edu.au

Adaptive Optics Systems VI, edited by Laird M. Close, Laura Schreiber, Dirk Schmidt, Proc. of SPIE Vol. 10703, 1070324 · © 2018 SPIE
CCC code: 0277-786X/18/$18 · doi: 10.1117/12.2314085

1.1 Instrument Overview

The ULTIMATE-Subaru project will develop wide-field near-infrared imager and multi-object spectrograph assisted by ground-layer adaptive optics (GLAO) system as a Subarus next facility instrument. Figure 1 shows the schematic overview of the ULTIMATE-Subaru subsystems. The GLAO system consists of an adaptive secondary mirror (ASM), four laser guide stars (LGSs) launched from the side of the telescope, four LGS wavefront sensors, and three or more natural guide star wavefront sensors for low-order tip/tilt and focus correction. The existing secondary mirror will be replaced by an ASM with ~ 1000 actuators. Baseline specification of the ULTIMATE-Subaru GLAO system is summarized in Table 1. One of the unique capabilities of the ULTIMATE-Subaru is a large field coverage area of up to 20 arcmin in diameter. Figure 2 shows the vignetting at the Cassegrain and Nasmyth focus of the telescope. At the Cassegrain focus, we found that the maximum 20 arcmin diameter field-of-view (FoV) can be obtained with less than 20% vignetting by removing the peripheral optical/mechanical components of the telescope, such as atmospheric dispersion corrector, slit viewer, calibration light source, and auto-guider and Shack-Hartmann camera for primary mirror analysis. Since such components are not necessary for the ULTIMATE-Subaru, we will remove them to get the maximum FoV. The patrol field of regard of the wavefront sensors will be at outside of the science FoV, which is 14×14 arcmin^2 where the vignetting is less than 10%. At the Nasmyth focus, the field coverage is ~ 14 arcmin in diameter, which accommodates $\sim 10 \times 10$ arcmin^2 science FoV. The Nasmyth has a bit smaller FoV than the Cassegrain mainly because of the vignetting by the tertiary mirror. Both of the platforms can be used for the GLAO assisted wide-field instruments.

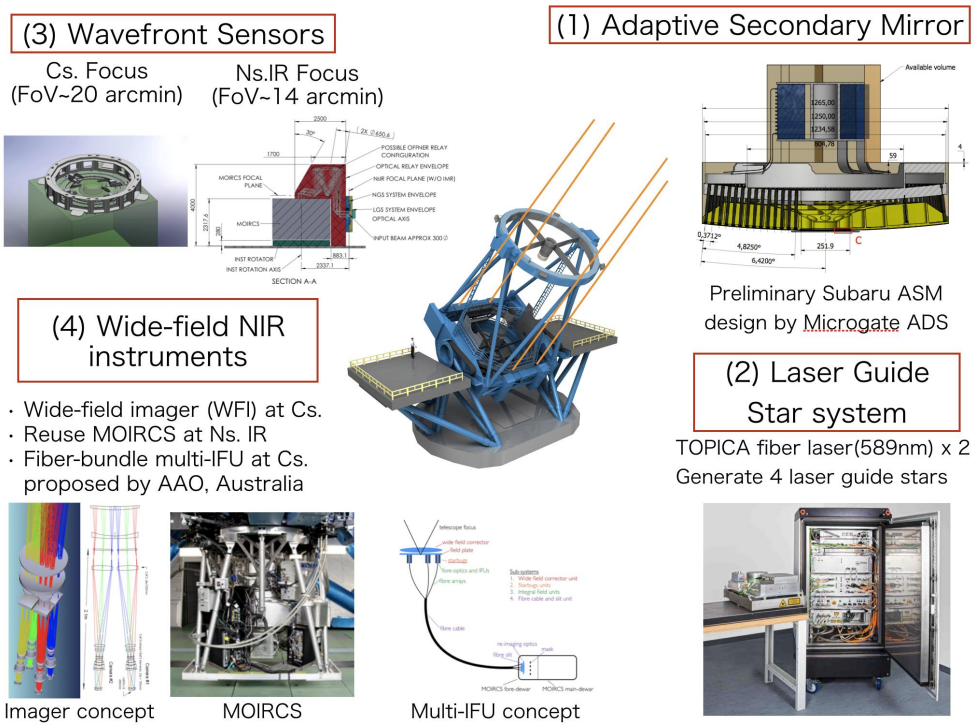

Figure 1. A schematic view of the ULTIMATE-Subaru subsystems required for the GLAO and wide-field near-infrared instruments.

We have been conducting conceptual studies of the ULTIMATE-Subaru NIR instruments: wide-field imager, multi-object slit (MOS) spectrograph, and multi-object integral field unit (IFU) spectrograph, which fully utilize the capabilities of the GLAO corrected spatial resolution and the wide FoV. We are considering the possibility to reuse the existing wide-field multi-object imager and spectrograph MOIRCS[4] at the Nasmyth platform as a first light instrument for the ULTIMATE-Subaru. We are also considering a new wide-field NIR imager (WFI) at the Cassegrain focus, which has 14×14 arcmin^2 science FoV, as a workhorse instrument for a large near-infrared imaging survey program with the ULTIMATE-Subaru. To fulfill the requirement from the science cases with

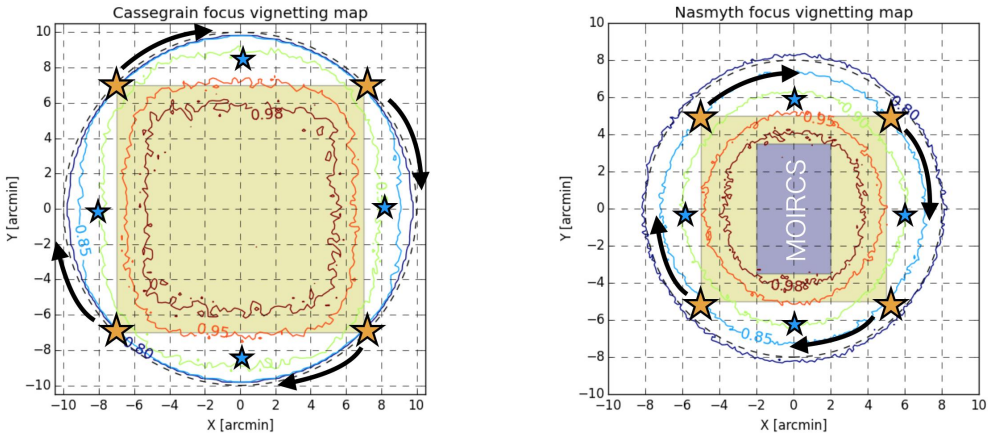

Figure 2. Vignetting map at Cassegrain and Nasmyth foci of the Subaru telescope. ULTIMATE-Subaru will cover $\phi \sim 20$ and ~ 14 arcmin field of view by GLAO, which contain $\sim 14 \times 14$ and $\sim 10 \times 10$ arcmin^2 science field of view, respectively. Orange and blues stars around the science field of view show the laser and natural guide stars, respectively.

Table 1. GLAO baseline specification

Item	**Specification**
Guide Star	4 LGSs ($\sim$ 10 W for each, $\sim$ 500 photons/cm^2/sec)
	4 NGSs ($r < 19$mag)
Technical FoV	LGS: edge of FoV ($r < 10'$ at Cs, $r < 7'$ at Ns)
	NGS: 4 crescent areas at the outside of science FoV
WFS	LGS: 32×32 Shack-Hartmann (0.″6/pix)
	NGS: 2×2 Shack-Hartmann (Visible, 0.″15/pix)
WFS frame rate	$>$ 500 Hz
Deformable mirror	Adaptive Secondary with $\sim$ 1000 actuators

the ULTIMATE-Subaru, we are planning to install a wide-variety of narrow/medium band filters especially in K band as well as regular broad-band filter set ($YJHK$) in NIR. The conceptual design of the multi-object IFU spectrograph (M-IFU) has been conducted in collaboration with Australian Astronomical Observatory (AAO).[5] The conceptual design assumes 8−13 fiber bundle IFUs with 1.18×1.18 arcsec^2 FoV for each, which are attached underneath of the wide-field corrector optics installed at the Cassegrain focus and are deployable anywhere on the focal plane at the Cassegrain focus using robotic positioners, called Starbug, developed by AAO. The fibers from the IFUs will be connected to any near-infrared spectrograph, although we consider MOIRCS spectrograph mode in the conceptual study. If we feed the light from the Starbug positioners into PFS spectrographs, which consist of 4 fiber-fed spectrograph modules with 2,394 optical fibers, we can increase the number of the IFUs up to ~ 40. Baseline specifications of the science instruments are summarized in Table 2.

Table 2. Baseline specifications for the ULTIMATE-Subaru science instruments

	MOIRCS	WFI	M-IFU
Wavelength coverage	0.9−2.5 μm		0.9−1.8 μm
Pixel scale	0.116 arcsec/pix	∼0.10 arcsec/pix	0.15 arcsec/spaxel
Field of view	$4' \times 7'$	$14' \times 14'$	IFU: $1.2'' \times 1.2''$ Patrol area: $14' \times 14'$
Spectral resolution	500−3000	–	500−3000
Multiplicity	40−60 slits	–	8−13 IFUs
Detector	2×H2RG	4×H4RG	2×H2RG
Efficiency	15(J), 20(H), 26(K)%	> 40%	9(J), 12(H)%

1.2 Science Case

The wide-field survey power and multiplicity together with the high spatial resolution achieved by ULTIMATE-Subaru allows us to conduct unprecedentedly deep and wide-field NIR extra-galactic survey (Figure 3). This is an essential step for us to prepare for the era of 30m class telescopes by having our original targets to follow up with. In particular, ultra-deep, wide-field narrow-band and medium-band imaging will be the most unique part of the ULTIMATE-Subaru. Narrow-band imaging will allow us to find very distant galaxy candidates at $z > 8$ based on Lyα emission. This is a direct extension of the current Subaru science with HSC towards more distant universe. Narrow-band imaging with high spatial resolution will also tell us where in galaxies they are forming new stars, how the star-forming activity propagates with cosmic times, mass, and environment. We note that the future wide-field NIR space missions (e.g., WFIRST) do not cover $\lambda > 2.0$ μm, and therefore ULTIMATE-Subaru can largely complement those space missions by conducting large survey in K band. By splitting the K band into three medium bands, we can select Balmer break galaxies to the $z \sim 5$, which will revolutionize our understanding of the distant universe currently explored with rest-frame UV light alone. Deep spectroscopic survey of high-z galaxies ($1 < z < 3.5$) at K-band is also unique, and kinematics along the slits based on the line profiles and velocity offsets will tell us how the turbulent disks and galactic central bulges are formed, and star formation is quenched. Furthermore, multi-object IFU survey assisted by GLAO for a large sample of galaxies at the cosmic noon will tell us the internal physical properties such as spatial distributions of dust extinction, ionizing states and gaseous metallicities for a statistical sample of galaxies for the first time, providing a unique kinematic survey capability at distant universe ($z > 1$) like MANGA[6]/SAMI[7] surveys at $z \sim 0$. In addition to the high-redshift galaxy science, the expected performance of ULTIMATE-Subaru will also be useful for a wide variety of science cases for nearby galaxies ($z < 0.3$), the Galactic center, globular clusters, and Galactic star-forming regions.

2. PERFORMANCE SIMULATION

After initial and extensive discussions to agree on atmospheric turbulence conditions, as well as agreeing on simulation parameters and input conditions baseline, the simulations effort was split in three stages:

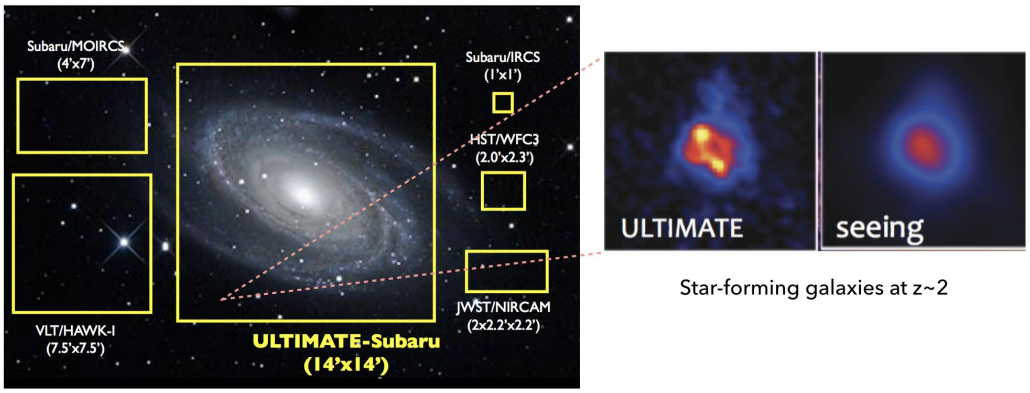

Figure 3. Comparison of the field of view at the current and future near-infrared imagers accessible to $\lambda > 2.0$ μm. ULTIMATE-Subaru will provide the widest field of view with the spatial resolution capable of resolving the internal structure of galaxies at high-redshift ($z \sim 2$).

1. **Stage 1: System design optimisation**: During this stage, a number of system parameters, were optimised to give the best system performance. This is the most labour intensive stage of the simulation. Fixed system parameters to be used were defined and included telescope characteristics, ASM, LLT, Number of LGSs, Na Laser, etc. Parameters to scan/optimise during stage 1 were decided upon an include the LGS and NGS WFS order, pixel size, field of view, sample rate, as well as the NGS WFS configuration (now many), type (SH vs Pyramid) and operating wavelength (visible vs NIR).

2. **Stage 2: Final system design performance**: The system design parameters determined during stage 1 are to be used during stage 2. The system performance was evaluated over a wide range of configuration (e.g. zenith angle, LGS asterism clocking, etc). Parameters to scan to produce these final performance included Zenith angle, asterism clocking, and include a estimating performance at various wavelength (YJHK).

3. **Stage 3: Full statistical performance predictions**: Based on a set of actual target, statistical distribution of the Sodium return, and database of Cn2 profile, many performance points were evaluated and presented in probability distribution for the various metrics. This is the most computer intensive stage of the simulations.

2.1 Simulation tools and infrastructure

Yao[8,9] was used for all end-to-end Monte-Carlo simulations. Yao has been around since 2000. It has been tested against many other simulation tools, has been used to dimension many AO systems and is arguably the most commonly used AO simulation package for small to medium size systems (new needs for ELT systems are changing the game however). It can simulate all that ULTIMATE-Subaru is likely to encompass: LGSs, SHWFSs, ASM, Ground Layer AO, etc. One modification had to be made to yao to include simulation of the field-dependent pupil vignetting at the Subaru Cassegrain focus.

Because of the breadth of the envisaged simulations (eventually, we reached 23000 hours of CPU time, which is almost 3 years of a single computer running 24/7), we needed access to a bank of computers. It was decided that using cloud computing services was the best solution, and we opted for Google Computing Engine, a cloud-based computing farm similar to AWS (Amazon Web Services). This solution was entirely satisfying, providing a scalable (up to 128 Virtual Machine running concurrently), convenient (a library and APIs are provided to manage the instances from the local computer) and inexpensive solution*. Virtual machines ("instances" in GCE parlance) and their environment (disks, etc) can be controlled through web-based panels or from the conveniency of the command line, using a set of command line tools provided by google, together with APIs.

2.2 Input conditions

Table 3 presents the Cn2 profiles we used in the simulations. They are essentially the ones used in,[10] which were based on Chun,[11] modified to adjust for an additional dome and ground layer due to (a) the Subaru site being lower and (b) the presence of a dome.

Table 3. MK C_n^2 Oya2014,[10] modified CHUN GL, 8 layers.

Alt [m]	C_n^2 25% [$m^{1/3}$]	C_n^2 50% [$m^{1/3}$]	C_n^2 75% [$m^{1/3}$]
0	1.766E-13	2.924E-13	4.031E-13
15	5.798E-14	5.007E-14	8.773E-14
30	2.155E-14	1.754E-14	1.537E-14
60	7.311E-15	1.279E-14	1.853E-14
119	2.626E-15	6.281E-15	2.050E-14
353	2.171E-14	4.132E-14	7.964E-14
1500	9.804E-15	2.348E-14	6.452E-14
9333	6.022E-14	8.385E-14	1.242E-13
Total	3.578E-13	5.277E-13	8.136E-13
r0(500cm) [cm]	14.9	11.8	9.1

2.3 Convergence analysis

Because we are using end-to-end, Monte-Carlo simulations, there is statistical noise associated with it. Obviously, to get meaningful results, we want to make sure we run enough iterations to reduce this statistical noise, or at least have an estimate of it. Figure 4 reports the results of convergence runs in term of performance (data points are FWHM and error bars are FWHM rms over the field) versus the number of iterations in the simulation run. The left figure is for a seeing limited run, the right one for a GLAO corrected one. One can draw several conclusions from these figures:

- Runs with too little iterations underestimate the average FWHM. That is expected, as a small number of independent realisations will mean that, (a) low aberrations like Tip-Tilt will not have gone through their whole amplitude and (b) there is more speckles, thus the maximum of the image is artificially high, thus biasing the FWHM toward smaller values, so that this **convergence noise** is in fact primarily a **convergence bias**;
- The closed-loop case converges significantly faster than the open loop case (typically 5000 versus 20000 to be within a few percent of the fully converged case). Again, an expected behaviour, as GLAO will

*Pre-emptible VMs – i.e. that can be interrupted by Google on 30 seconds notice – only cost $0.01 an hour, which turned out really handy as in our experience the VMs were interrupted less than 5% of the time. To this, one has to add the cost of storage and moving data around between nodes whenever necessary. Our overall bill was AUD800 for 23000 CPU hours.

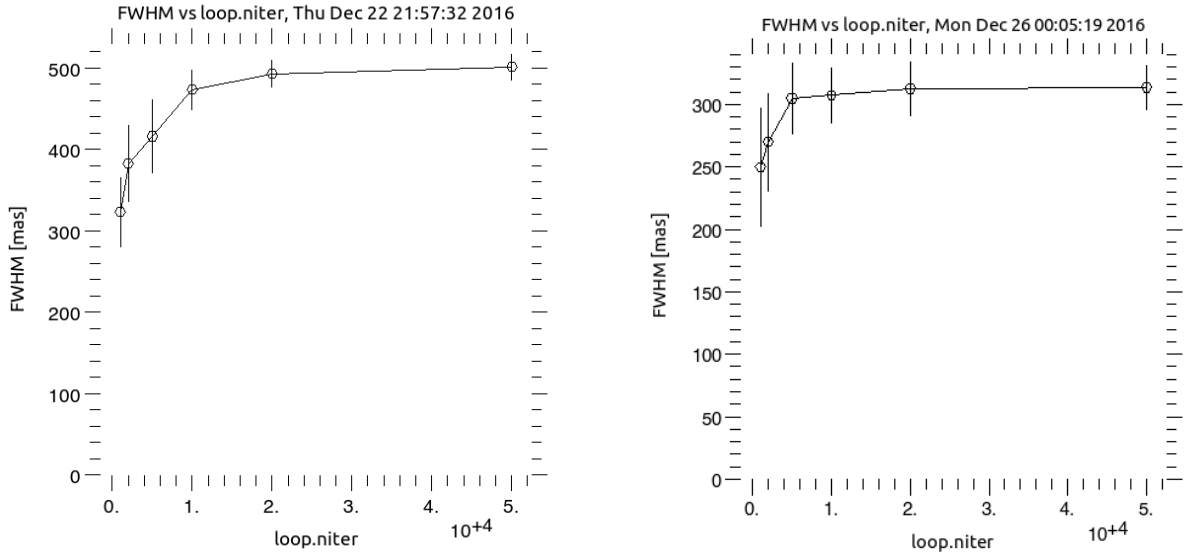

Figure 4. Evolution of the FWHM averaged over the field of view ($14' \times 14'$) versus the number of iterations in the simulation run. Left: Open-loop run (seeing limited). Right: Closed-loop run (GLAO). The error bars indicates the rms FWHM over the field of view (only 3x3 PSF in the corrected field). One can see that because of the contribution of the low spatial/temporal frequencies, the open loop case does not reach convergence as fast as the closed loop (20000 versus 5000 iterations).

compensate for part of the low order aberrations (addressing (a) above) and will reduce the number of speckles (addressing (b) above);

- A not-large-enough number of iterations also affect the rms over the field of view, as evidenced by the larger error bars (as said above, error bars trace the rms over the field of view).

2.4 Impact of the field of view

It has been shown by several authors[12] that the altitude depth of influence of a DM for the high order aberrations is

$$\Delta h = \frac{d}{\theta}$$

where θ is the field of view and d the DM pitch. The wider the field of view, the narrower the equivalent depth of the corrected layer. At the extreme, if the field is infinitely large, the depth of the slab of atmosphere corrected is essentially zero. Opposite, if the field of view is very narrow, then a single DM can correct the whole atmosphere (as in classical AO). The figure 5 reports on simulation of GLAO FWHM performance versus the size of the field of view (here equal to the side of the square LGS asterism) for the various seeing Cn2 cases (25, 50 and 75%). On the left are the absolute FWHM, on the right the FWHM gain from seeing limited to GLAO corrected. This was before we corrected a bias in the phase screen normalisation, so the FWHMs are pessimistic by a approximately 25% (both seeing and GLAO corrected). The main conclusions from these figures is that:

- The FWHM gain plateaus at 2 even for large field of view.
- However, the FWHM gain can be much larger (up to 4 and more) when the field of view is reduced down to 3 arcmin or less.
- intermediate fields provide intermediate gains.

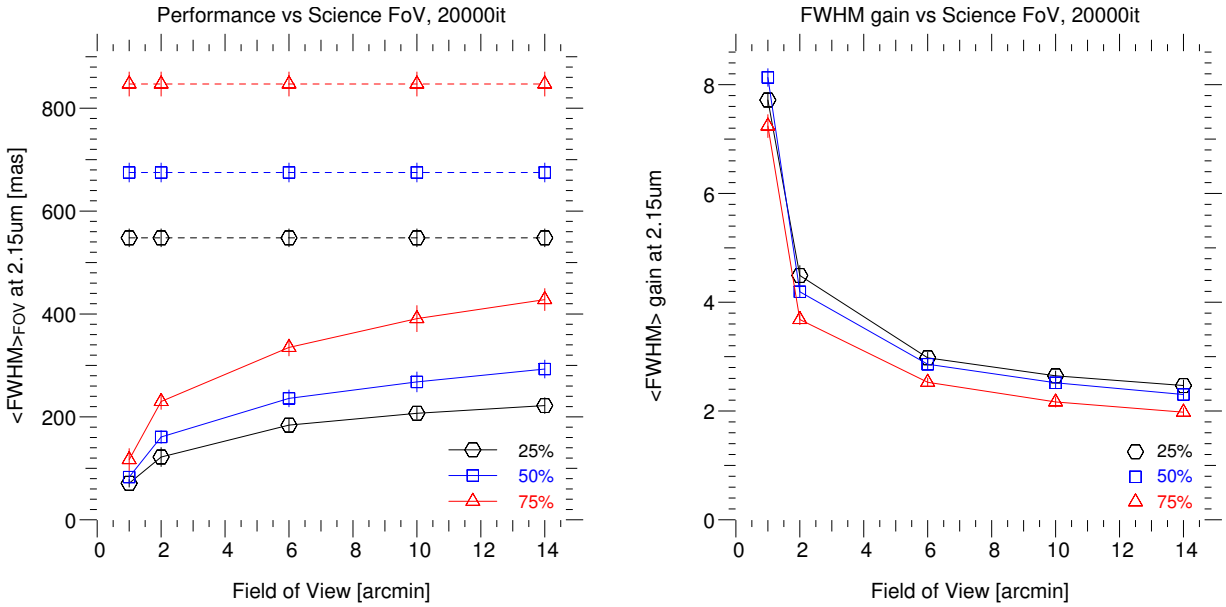

Figure 5. GLAO FWHM performance as a function of the field of view (side of the LGS asterism) for the selected 25%, 50% and 75% Cn2 profiles. Left: absolute performance with (lower curves) and without (upper curves) GLAO. Right: improvement GLAO over seeing limited. Note that this was done before the phase screen normalisation adjustment, so that the absolute level of the curves in the left panel curve is off.

This calls for the system **to be able to change its constellation diameter to adjust to the science program field of view needs**. Although most ULTIMATE-Subaru currently defined science cases are geared to use the $14' \times 14'$ field, it is likely that, ULTIMATE-Subaru being a facility instrument, many new applications will make use of a smaller field; having the ability to adjust the constellation size – if its implementation is neither too costly nor too risky – to tailor to the science need will always insure that the best performance is delivered to the science program.

Making sure that this makes it into the design specification of ULTIMATE-Subaru also provides an insurance against instances of Cn2 profile that would be less favourable than the one (carefully) adopted for these simulations. If ever the Cn2 is bias toward slightly higher altitudes, having the ability to adjust the Fov will make an important different in performance.

2.5 Stage 1 and 2: System design simulations

This section describes the simulations we have made to determine optimal parameters for the ULTIMATE-Subaru GLAO system: LGS and NGS detector pixel sizes, WFS framerates, as well as a first order performance characterisation. The optimisation of the LGS and NGS WFS parameters was done independently. We first neglected the NGS errors to optimise the LGS WFS parameters and then use these parameters to optimise the NGS WFS ones.

To determine the optimal LGS WFS, we ran simulations probing the following parameters:

- Seeing conditions (25, 50 and 75 percentile cases)
- Controller loop gain (0.2, 0.4)
- Frame rate (200, 400, 600 Hz)
- LGS flux (0 - 250 ph/s/cm^2)
- LGS WFS pixel size (0.4 - 1.0")

- Number of SH-WFS subapertures (26×26 and 32×32)

We are baselining a S-CMOS detector for all LGS WFSs; in particular an ORCA FLASH 4.0. Of all the characteristics of this detector, the one relevant for the current optimisation is the noise (1.2e- RMS), and the maximum read out rate the one set by the line read out time of $4.88\mu s$ (so that, for example, reading out a ROI of 256 lines high takes 1.25ms, leading to a maximum frame rate of 800Hz[†]). All of these conditions were folded in the simulations.

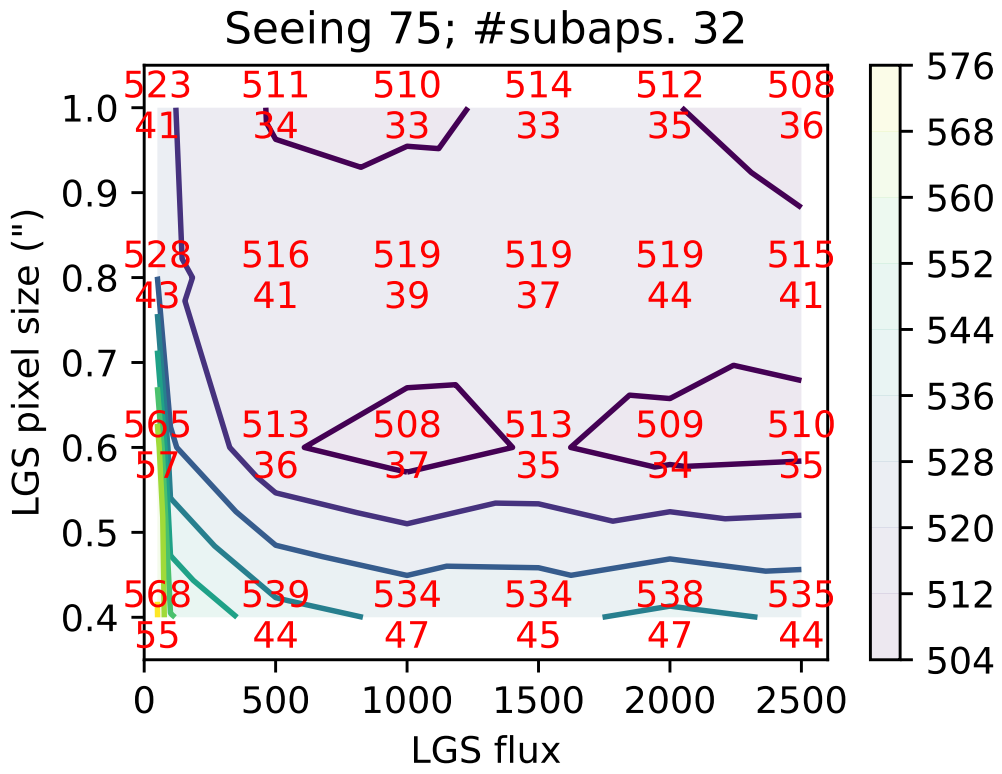

Figure 6. Averaged FWHM as a function of LGS flux and pixel size. The LGS flux units are in ph/s/cm^2 at M1.

Fig 6 shows the GLAO-corrected FWHM for the worse seeing case (75%). The optimal FHWM is not strongly dependant upon the LGS flux or the LGS pixel size; only at the flux levels lower than about 250 we can see the that the larger pixels (over 0.6") are more beneficial as compared pixels of 0.6" and smaller. In the strongest seeing case, with flux levels deemed realistic (over 500), the pixel size of 0.6" seems to be optimal. In the median and good seeing case, pixel sizes of 0.6-1.0" give essentially the same results with flux levels larger than 200. We adopted the value of 0.6" for the LGS WFS pixel size.

For the NGS pixel size, because corrected images are expected to have FWHMs of about 0.2" at the best seeing level (25%), the case could be made that the ideal NGS WFS pixel size should be 0.1" (Nyquist). However, SNR considerations may drive this to larger value, to increase the collected flux. One known issue in centroid determination when enlarging the pixel size is that too large a pixel size may bias the centroid measurement when the spots are not exactly centred between (at the corner of) 4 pixels. Thus the purpose of the numerical simulations is to find the optimum between SNR and loss of performance due to estimation bias. We ended up selecting a value of 0.15" per pixel.

[†]Note that these frame rates are achievable only in rolling shutter mode, which by itself opens a whole series of interesting issues.

Eventually, nominal performance can be simulated with these baseline system parameters. The following mean FHWM values are obtained for seeing-limited and GLAO corrected images:

Seeing case	<FWHM>$_{\mathrm{FOV}}$, seeing limited	<FWHM>$_{\mathrm{FOV}}$, GLAO
25%	343 mas	148 mas
50%	443 mas	208 mas
75%	578 mas	320 mas

For median seeing, the GLAO-corrected FWHM of 0.2" is perfectly in line with.[10,13]

2.6 Stage 3: Full statistical performance set-up

This section describes the simulations carried out to evaluate the long-term performance of the ULTIMATE-Subaru GLAO system, over all possible conditions of seeing, pointing, Sodium column density and sky background.

We used the optimal design parameters for LGS and NGS WFSs described above. The control system was moderately well optimised: frame rate and gain were selected optimal for median conditions (frame rate of 600 Hz, high-order loop gain of 0.2 and tip/tilt mirror loop gain of 0.8×0.2). No effort was made to optimise the tip/tilt correction using appropriate weighting to take into account the differences in NGS brightnesses.

Cn2 profile and timestamp: We used site monitoring data from the Maunakea site monitoring campaign.[11] These data were collected using a combination of site testing instruments on the roof of the UH2.2 m, located on the Maunakea ridge, elevated 80 m above Subaru site and a few hundred meters away. The dataset contains over 26000 unique profiles covering a time period of almost two years. We averaged individual profiles over periods of about 26 mn to create 1001 Cn2 profiles. Identical times and dates of year as the ones at which the Cn2 profiles were obtained were chosen for the simulated observations. Finally, we adjusted the binned profiles such that the median seeing computed from all the Cn2 profiles was equal to our simulation 50 percentile seeing (Fried parameter r_0 at 500 nm was 11.8 cm). This was done by adding a constant contribution to the ground layer, which physically is justified by the fact that the most likely assumption is that the free atmosphere is identical between the UH2.2 and the SUBARU site; what changes is the ground and dome layer.

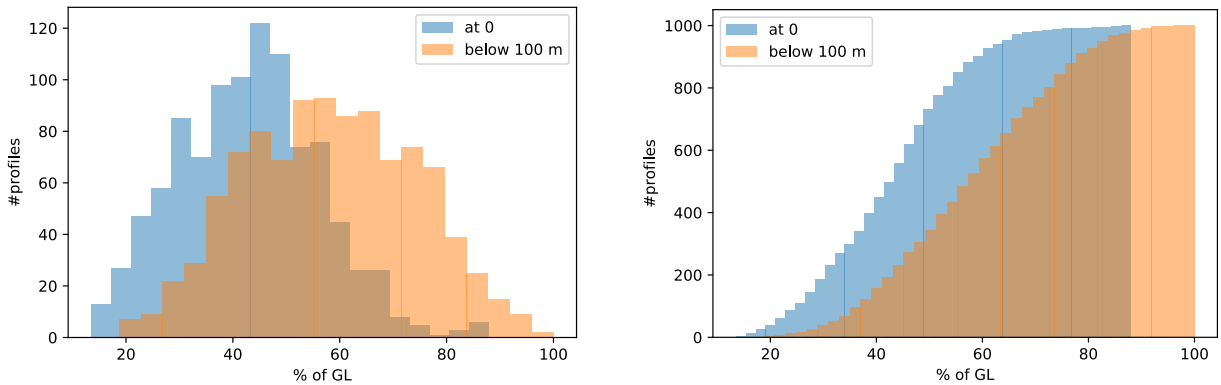

Figure 7. Histograms illustrating the distribution of turbulence in the binned profiles: percentages of turbulence in the ground layer (0 m and below 100 m).

Pointing and NGS asterism: Every binned profile is associated with a UT and a date of year (the UT and date of year of the profile in the Chun database). This gives us a Sidereal time at Maunakea for each profile. Next, we created a random pointing; The zenith angle is chosen to follow the probability distribution drawn from engineering data from years of pointing statistics at the Subaru telescope. The azimuth angle of our pointing was chosen to follow the uniform distribution. Once the RA and DEC have been obtained following this

procedure, we used a catalogue to search for NGS asterisms for each pointing. The criteria for asterism selection was simple: we just selected the brightest star in each crescent, with an additional condition that the minimum distance between two guide star has to be larger than 1'. In general, because of the large area available for NGS selection (a crescent $10' \times 3'$), we had no issue finding bright guide stars (typically R<14).

Sodium column density: After literature review and discussions with different groups about the latest sky data, we decided to adopt 720 photons/cm^2/s per LGS at M1. Each TOPTICA laser is split to create two LGSs. We assumed 8W projected on sky and a median value of 90 photons/cm^2/s/W at M1. Note that, assuming 45% optical throughput and QE combined and a 32×32 subaperture system, that would translate into 213000 photons/s/subaperture (213ph/frame/subaperture at 1kHz). This median value was modified including a combination of seasonal variability (to which the observation date is an input), night to night and observation to observation variabilities, using an ad-hoc approach. The seasonal variation of Sodium has been studied by many authors. It is latitude and hemisphere dependant. For the seasonal variations, there are various reports from Sodium measurement campaigns that can be found in the literature, although none for Maunakea. Roberts[14] reports on measurement made at Maunaloa (same latitude, very close to Maunakea). A fit of the data reported by Roberts gives a seasonal variation of the sodium column density of the form $1 + 0.20 \times \sin(2\pi(d - 42)/365)$, where d is the day of year. For the night to night and observation to observation variability, we just assumed uncorrelated, log normal probability density functions each with a rms of 1.44. Last but not least, we introduced the sodium return variation due to pointing (therefore using the elevation and azimuth as described above), as described by Holzlöhner.[15]

Sky Background: Because the ULTIMATE-Subaru science is primarily in the NIR, the observation will most likely be primarily in bright time. Thus, instead of using the moon phase of the date-of-year, we draw a random moon phase comprised between 50% and 100% bright time.

For each 1001 unique settings we then evaluated both GLAO and seeing limited performance. In the following, we present the simulation results.

2.7 Stage 3: Full statistical performance results

Figure 8 shows the FWHM as a function total Cn2 at the zenith angle for the simulated observations. For GLAO simulations, the plot colour encodes the percentage of turbulence that is located below 60 m. Note that the scatter of the seeing limited points (red) is due to convergence noise in the simulations (5000 iterations). It measures at approximately 50mas. The plot shows that there is a very large scatter for the GLAO corrected FWHM, with the best improvement obtained when the fraction at ground is the largest (unsurprisingly). Another, even clearer way to demonstrate this is shown in the right panel. We have plotted the ratio of GLAO FWHM to seeing limited FWHM as a ratio of the fraction of turbulence below 100 m. Once more, unsurprisingly, there is a very clear correlation (with almost a linear relation) showing improved performance when there is more turbulence at the ground.

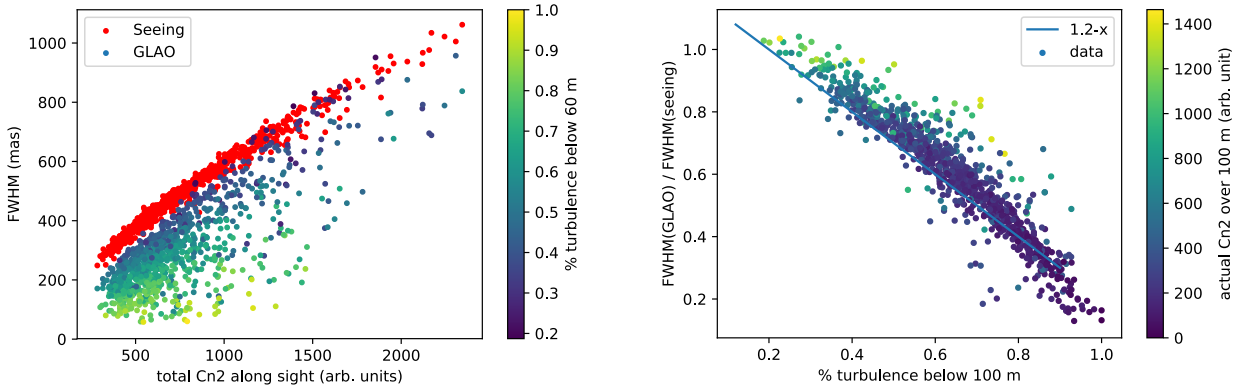

Figure 8. Left: Scatterplot showing seeing limited and GLAO corrected FWHM as a function of total turbulence. The colour of the GLAO points encode the fraction of turbulence below 60 m. Right: GLAO correction ratio (ratio of FWHM GLAO to seeing limited) as a function of the fraction of turbulence below 100 m.

Finally, Fig 9 presents the histogram of FWHMs, with GLAO (orange) and seeing limited (blue), as well as the cumulative histogram version (right), which shows an improvement of close to, but not quite a factor of two in the histogram median. This shows the benefit of running detailled simulation using real-world conditions with respect to the Stage 1 and 2 simulations, that were using only 3 profiles and fixed conditions (zenith angle, sodium return etc). We are still in the process of reconciling these two results.

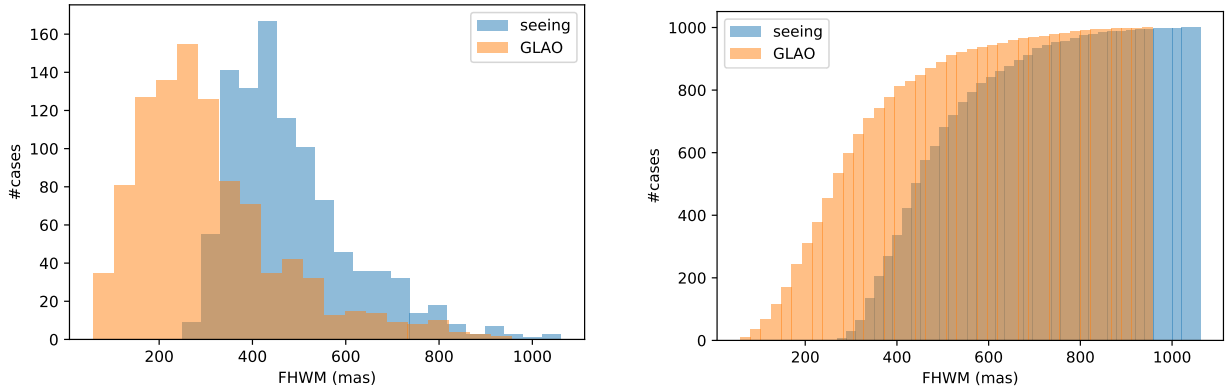

Figure 9. Histogram of all GLAO and seeing-limited FWHMs resulting from stage 3 simulations. Right: same, in the form of a cumulative histogram.

3. WAVEFRONT SENSORS CONCEPTUAL DESIGN

A GLAO system using a deformable secondary can drastically reduce the number of optics in the science path. This is the philosophy we have been using in the design of ULTIMATE-Subaru GLAO. The AO module is just made of a focus adaptor (WAF = Wavefront Adaptor Flange), hosting the LGS and the NGS WFSs in a narrow flange interfacing the telescope with the instrument as shown in Fig 10. The same design has been used for Cassegrain and Nasmyth (latter not shown).

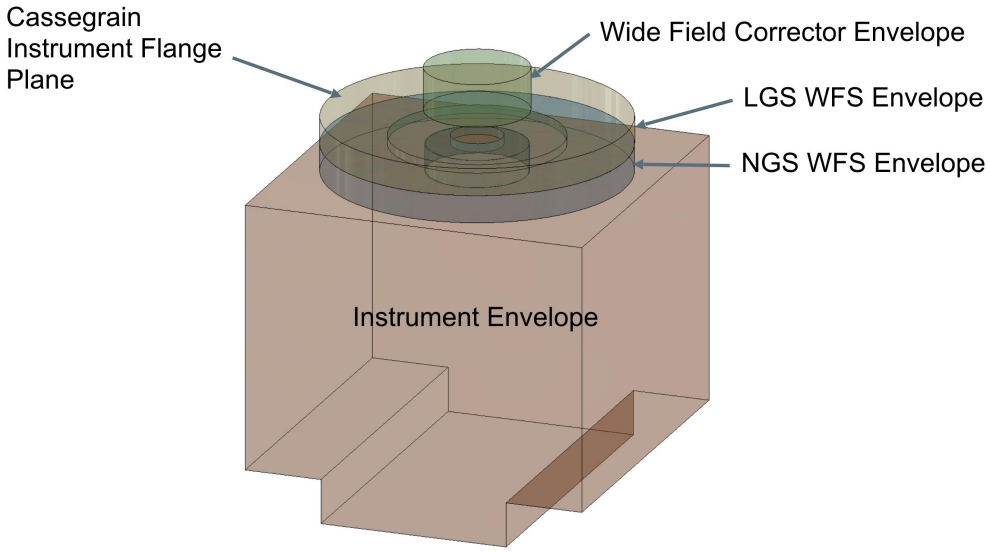

Figure 10. Wavefront Sensor Adaptor Flange, showing the Wide field corrector (located inside the cassegrain volume above the Cassegrain instrument interface plate), as well as the WAF, sandwiched between the Cassegrain interface and the instrument.

Fig 11 shows details of the design inside the WAF. The top part if the LGS WFS assembly. This stays fixed (does not rotate) with the telescope; both the changing range to the LGS (typically from 80 to 200km) and the

variable constellation diameter can be adjusted/compensated by moving the green plate and the yellow probe as shown in figure 12 (stage under the probe is not shown).

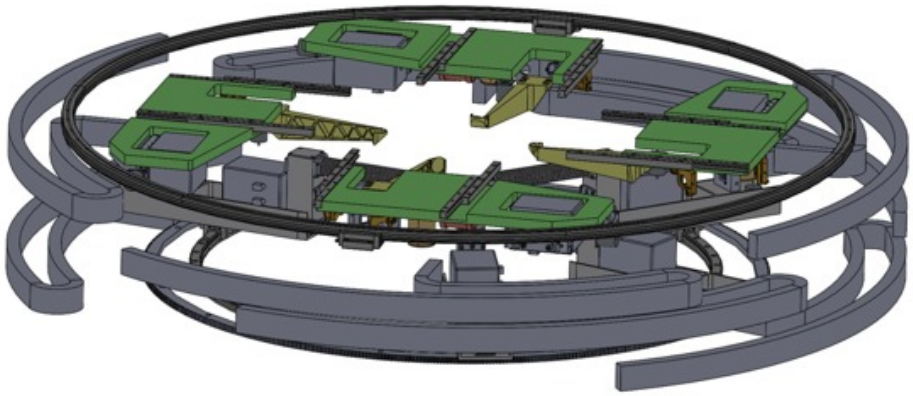

Figure 11. Wavefront Sensor Adaptor Flange, with the LGS WFS assembly on top (including the green stages), and NGS WFS assembly on the bottom. The LGS WFS are detailled below. The NGS WFSs are on circular rail and can extend in/out to select NGSs. They can even protrude inside the science field in case there is no NGS available in the crescent patrol region, or in case of operation with a reduced science field of view.

The NGS WFSs, in this configuration, will sometimes be vignetted or even totally obscured as the NGS WFS assembly rotates with respect to the LGS WFS assembly. This is unavoidable. We are planning to have four NGS WFSs to reduce the impact of this problem. NGS WFS guide stars can be changed on the fly if necessary, or observations (guide star selection) can be planned to reduce the number of vignetting occurrences.

4. SUMMARY AND FUTURE PROSPECTS

ULTIMATE-Subaru is a next large facility instrument program at Subaru telescope, which will provide 14×14 arcmin^2 wide-field near-infrared imaging and multi-object spectrograph capabilities with the aid of ground-layer adaptive optics system (GLAO). Currently, Subaru is conducting conceptual design and feasibility studies of the GLAO system for the ULTIMATE-Subaru in collaboration with the Australian National University, Tohoku University and ASIAA. Design parameters of the GLAO system were optimized using end-to-end performance simulations. The GLAO performance simulations showed that ULTIMATE-Subaru can reduce the FWHM by $\sim 50 - 60\%$ in all seeing conditions. Median FWHM after the GLAO correction is about 0.2 arcsec in K band. This result is promising for future wide and high-spatial resolution NIR survey with ULTIMATE-Subaru. We also conducted optical and mechanical conceptual design of the wavefront sensor systems at the Cassegrain and Nasmyth platform of the Subaru telescope. The next milestone for the ULTIMATE-Subaru project is to have a conceptual design review of the GLAO system in early October, 2018.

We are aiming to have engineering first light of the GLAO in 2025 and start the science observation with the GLAO in 2026. In addition to the conceptual design, we are also conducting the upgrade of the existing facility AO system (AO188) at the Subaru telescope to develop fundamental technologies for the ULTIMATE-Subaru GLAO system.[16] Currently, we are developing a new real-time control system for AO188 that will be able to use for the future GLAO system.[17] The TOPTICA fiber laser (589 nm) system, which will be used for the GLAO system as well, has been delivered to the Subaru telescope for upgrading the current LGS facility used

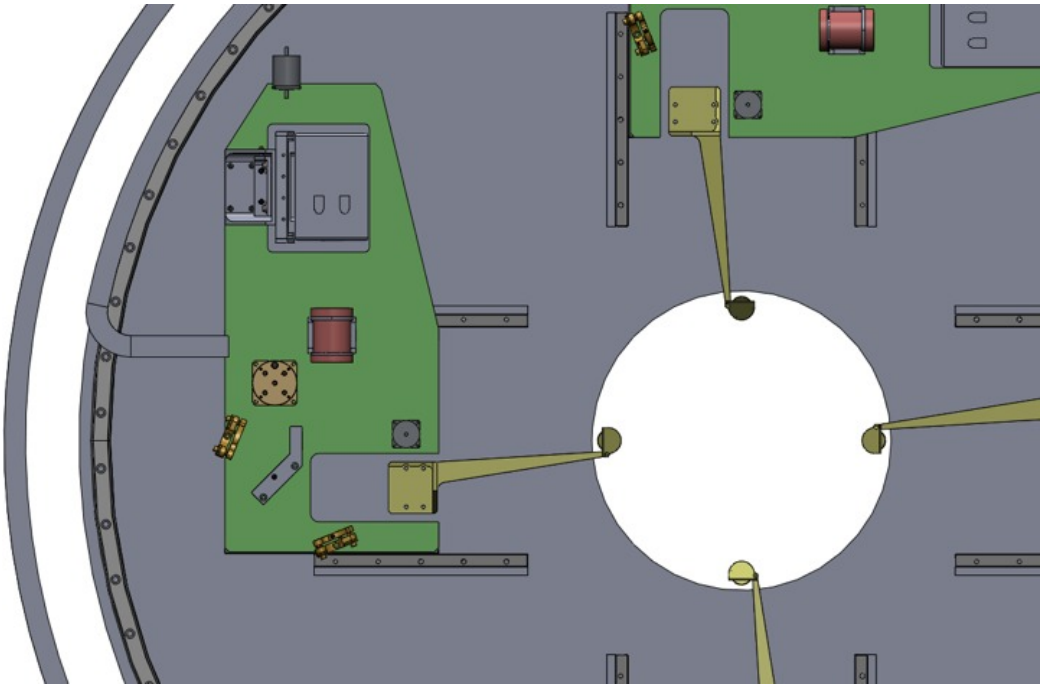

Figure 12. Wavefront Sensor Adaptor Flange, showing the Wide field corrector (located inside the cassegrain volume above the Cassegrain instrument interface plate), as well as the WAF, sandwiched between the Cassegrain interface and the instrument.

by AO188 in LGS mode. We are going to develop laser beam diagnostics and steering system so that we can use the same system for the future ULTIMATE-Subaru GLAO system.[18] We are also planning to implement a laser tomographic AO (LTAO) mode in AO188 to improve the performance of AO188 especially in optical wavelength and to demonstrate tomographic wavefront reconstruction with multiple laser guide stars, which is also essential for the ULTIMATE-Subaru GLAO system.

ACKNOWLEDGMENTS

The development of ULTIMATE-Subaru is partly supported by the Japan Society for the Promotion of Science (Grant-in-Aid for Research #17H06129).The authors wish to recognize and acknowledge the very significant cultural role and reverence that the summit of Maunakea has always had within the indigenous Hawaiian community. We are most fortunate to have the opportunity to conduct observations from this mountain.

REFERENCES

[1] S. Miyazaki, Y. Komiyama, S. Kawanomoto, *et al.*, "Hyper Suprime-Cam: System design and verification of image quality," *PASJ* **70**, S1 (2018).

[2] N. Tamura, N. Takato, A. Shimono, *et al.*, "Prime Focus Spectrograph (PFS) for the Subaru telescope: overview, recent progress, and future perspectives," in *Ground-based and Airborne Instrumentation for Astronomy VI*, *Proc. SPIE* **9908**, 99081M (2016).

[3] ULTIMATE-Subaru working group & Science team, "ULTIMATE-Subaru Study Report 2016," (2016). http://www.naoj.org/Projects/newdev/ngao/20160113/index.html.

[4] R. Suzuki, C. Tokoku, T. Ichikawa, *et al.*, "Multi-Object Infrared Camera and Spectrograph (MOIRCS) for the Subaru Telescope I. Imaging," *PASJ* **60**, 1347–1362 (2008).

[5] S. C. Ellis, R. Zhelem, D. Brown, *et al.*, "ULTIMATE: a deployable multiple integral field unit for Subaru," in *Ground-based and Airborne Instrumentation for Astronomy VI*, *Proc. SPIE* **9908**, 99081Q (2016).

[6] K. Bundy, M. A. Bershady, D. R. Law, *et al.*, "Overview of the SDSS-IV MaNGA Survey: Mapping nearby Galaxies at Apache Point Observatory," *ApJ* **798**, 7 (2015).

[7] J. J. Bryant, M. S. Owers, A. S. G. Robotham, *et al.*, "The SAMI Galaxy Survey: instrument specification and target selection," *MNRAS* **447**, 2857–2879 (2015).
[8] F. Rigaut, "YAO Adaptive Optics simulation package." https://github.com/frigaut/yao (2002).
[9] F. Rigaut and M. van Dam, "Elt ao simulations on a laptop with yao," in *AO4ELT3*, (2013).
[10] S. Oya, Y. Hayano, O. Lai, *et al.*, "Ultimate-subaru: simulation update," in *SPIE Astronomical Telescopes+ Instrumentation*, 91486G–91486G, International Society for Optics and Photonics (2014).
[11] M. Chun, R. Wilson, R. Avila, *et al.*, "Mauna kea ground-layer characterization campaign," *Monthly Notices of the Royal Astronomical Society* **394**(3), 1121–1130 (2009).
[12] F. Rigaut, "Ground conjugate wide field adaptive optics for the elts," in *Beyond conventional adaptive optics*, **58**, 11 (2001).
[13] S. Oya, M. Akiyama, Y. Hayano, *et al.*, "A preliminary simulation result of the next-generation wide-field ao at subaru telescope," in *SPIE Astronomical Telescopes+ Instrumentation*, 84473V–84473V, International Society for Optics and Photonics (2012).
[14] L. C. J. Roberts, L. W. Bradford, C. R. Newman, *et al.*, "Measurements of mesospheric sodium abundance above the hawaiian islands," *Proc. Astron. Soc. Pacific* **119**, 787–792 (2007).
[15] R. Holzlohner, D. Bonaccini Calia, D. Bello, *et al.*, "Comparison between observation and simulation of sodium lgs return flux with a 20w cw laser on tenerife," in *SPIE*, **9909** (2016).
[16] Y. H. Ono, Y. Minowa, C. S. Clergeon, *et al.*, "Ongoing and future AO activities on Subaru telescope," in *Adaptive Optics Systems VI*, *Proc. SPIE* **10703** (2018).
[17] C. S. Clergeon, Y. Minowa, O. Guyon, *et al.*, "Subaru AO188 upgrade phase 1: integration of the new real-time system," in *Adaptive Optics Systems VI*, *Proc. SPIE* **10703** (2018).
[18] E. Mieda, Y. Minowa, C. S. Clergeon, *et al.*, "Current status of the laser guide star upgrade at Subaru telescope," in *Adaptive Optics Systems VI*, *Proc. SPIE* **10703** (2018).